Robotica (2017) volume 35, pp. 1906–1922. © Cambridge University Press 2016
doi:10.1017/S0263574716000576

Research on a multimodal actuator-oriented power-assisted knee exoskeleton

Yali Han*, Songqing Zhu, Zhou Zhou, Yu Shi and Dabin Hao

School of Mechanical Engineering, Nanjing Institute of Technology, Nanjing, China.
E-mails: zusongqing@126.com, 18662826611@163.com, 13512518837@163.com, hdb5151@163.com

(Accepted July 21, 2016. First published online: August 17, 2016)

SUMMARY
A multimodal actuator was proposed to achieve a more agile power-assisted exoskeleton in uncertain complex walking environments. A power-assisted knee exoskeleton prototype based on a multimodal actuator was constructed. With this multimodal actuator, several modes of operation in the power-assisted knee exoskeleton during a motion cycle are actuated, including series elastic actuation, stiff position control, and energy storage and release. Also, a control strategy for power-assisted knee exoskeleton motion control based on a state machine is developed. The ability of the power-assisted knee exoskeleton to follow human motion was tested, and the results showed that the angle error of the knee exoskeleton followed the human motion is not more than 0.4°, and the response time error of the knee exoskeleton followed the human motion is not more than 0.2 s.

KEYWORDS: Multimodal actuator, Power-assisted exoskeleton, Brake block, Motion modes, Series elastic actuator

1. Introduction

A power-assisted exoskeleton leg is an anthropomorphic mechanism capable of assisting the lower-limb motions. In recent years, different types of powered exoskeletons have been developed.[1–3] Their applications can be categorized into two types: (1) walking strength enhancement over a long distance or load augmentation to carry heavy load and (2) walking aids for gait disorder persons or aged people.

A load-carrying assist exoskeleton is typified by the BLEEX system was developed at UC Berkeley,[4] in which the exoskeleton supports a load carried by the user. This device is driven with a linear hydraulic actuator and employs a control scheme that enables it to closely track the human's movements via positive kinematic feedback. Jacobsen's Salt Lake City-based company, Sarcos, has developed another version of an exoskeleton suit.[5] This device is driven by a rotary hydraulic actuator. A person wearing the designed powered exoskeleton on his or her legs and arms can carry about 200 pounds of load and feel only 20 pounds. This exoskeleton could enable soldiers to haul heavier equipment over longer distances and rescue workers to carry survivors more safely. The biomechatronics group at MIT also developed an exoskeleton.[6] The joint components of the exoskeleton in the sagittal plane consist of a force-controllable actuator at the hip, a variable-damper mechanism at the knee, and a passive spring at the ankle. The control strategy is implemented based on angle and force sensor readings of the exoskeleton. And through the analysis of the dynamic and kinematic parameters of the human body during walking, the spring and damping coefficient of the exoskeleton are adjusted to achieve the goal of boosting. It is a lightweight, underactuated exoskeleton.

* Corresponding author. E-mail: s966237@163.com

A robotic training device for gait rehabilitation generally uses a partial body-weight support, assisting patients in re-learning walking movements through repetition and task-oriented training. These devices are widely known, such as Lokomat.[7] Bortole *et al.*[8] designed a rehabilitation robot called H2 which has strong robustness and security for stroke patients. The Active Limb Exoskeleton (ALEX), developed at the University of Delaware, is a motorized exoskeleton that uses motors at the hip and knee joints and the force of the foot to help in gait training.[9] Copilusi *et al.*[10] also designed a leg exoskeleton for motion assistance. Sankai *et al.*[11] developed the Hybrid Assistive Leg (HAL) for individuals with gait disorder. The HAL can provide assistive torques for the user's hip and knee joints according to the user's intention by using the EMG signal as the primary command signal. With the motor drivers, measurement components, control computer, wireless local area network (LAN), and power supply unit built in the backpack, HAL works as a completely wearable system. The system can also potentially enable soldiers, firefighters, disaster relief workers, and other emergency personnel to carry loads, such as foods, weapons, rescue equipment, and communication gears, with minimal effort over any type of terrain for extended periods of time.

Although significant advances have been made in the exoskeleton robot design, all of these robots are actuated and controlled using conventional engineering techniques and all meet the specific tasks with narrow performance goals. Therefore, a wide range of behaviors is necessary for autonomous exoskeleton robot in uncertain complex walking environments. Some researchers have developed variable stiffness actuators[12–20] for broadening the output impedance of actuator and have proven that these actuators are more beneficial for some applications, particularly for rehabilitation exoskeleton robots. Stiffness is not the only way to change the output performance of an actuator. The damping component,[21–24] is also applied in actuators to broaden their output performance. Derek *et al.*[25] proposed a linear multimodal actuator based on brakes and clutches for hopping robots.

In view of transmission mode on the power-assisted exoskeleton is single, so a multimode elastic actuator which possesses the eight different modes is designed. In this paper, an actuator that combines the motor, spring, brake, and clutch, producing multimodal actuation for a power-assisted knee exoskeleton is presented. Based on the small-sized brake block, which can generate relatively large holding forces, the actuator is capable of instantaneously switching between different modes, including stiff actuator and series elastic actuator. The actuator was tested on a statically mounted single-degree-of-freedom exoskeleton that performs knee flexion, foot striking the ground, foot bouncing off the ground, and knee extension. The testing of power-assisted knee exoskeleton following human motion was also implemented, and the performances of the actuator and knee exoskeleton were analyzed and discussed.

The remainder of this paper is organized as follows. Section 2 describes the mechanism and design of the multimodal actuator, and Section 3 describes the power-assisted exoskeleton platform. Section 4 provides the results of the motion experiments, and Section 5 concludes the paper and discusses direction for future research.

2. Design of the Multimodal Actuator

2.1. Design overview of the multimodal actuator

A multimodal actuator which can take advantage of multiple discrete couplings (i.e., brakes and clutches) is designed. The multimodal actuator has a motor as dynamic element, paired with a clutch at the center as the foundation. The central block can then be bypassed by the brakes acting in parallel. The motor and clutch allow the output to be actuated or passive. The multimodal actuator is capable of operating a joint with different mechanical characteristics by configuring the couplings. For example, a legged robot can use series elastic mode for fast running by storing energy in the spring, it also can use stiff position actuated mode for a precise control of leg when carrying large payloads.

In order to specify the torque and joint angle requirement for our multimodal actuator and power-assisted knee exoskeleton, biomechanics data of human with different backpack load during level walking and stair climbing[26] was studied. The multimodal actuator include of servo motor, screw-nut transmission mechanism, spring, guide rail, brake rail, and brake block, as shown in Fig. 1. The servo motor of the multimodal actuator is a Maxon RE DC motor with a power rating of 60 W and a continuous torque rating of 85 mNm. The motor features a proprietary emulated encoder with a resolution of 500 counts. The ball screw driven by the DC motor has a range of 200 mm, a diameter

https://doi.org/10.1017/S0263574716000576 Published online by Cambridge University Press

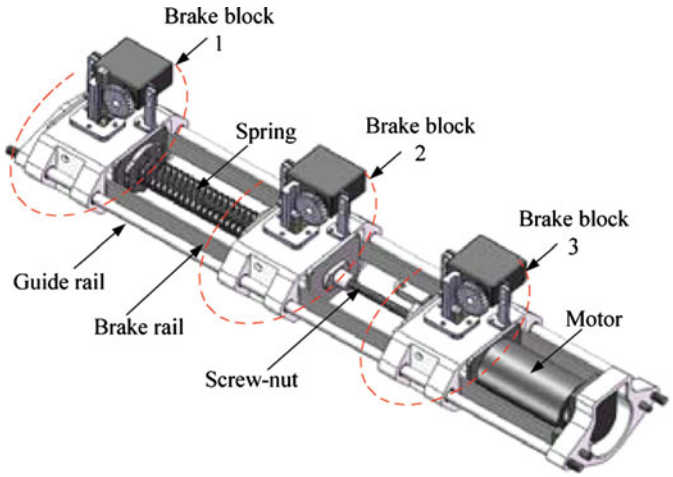

Fig. 1. Multimodal actuator.

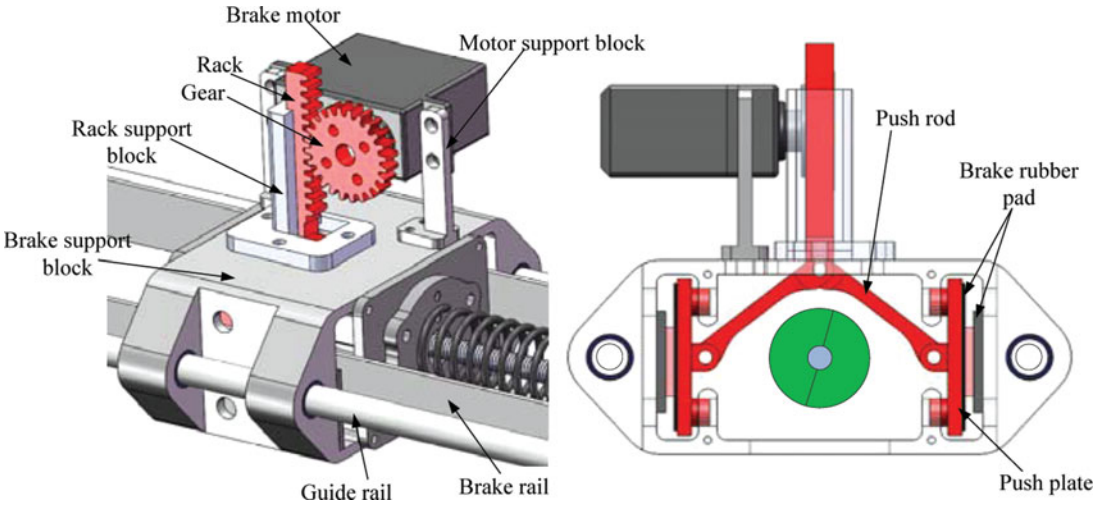

Fig. 2. Brake block mechanism.

of 8 mm, and a lead of 2 mm. The three brake blocks are mounted onto a pair of guide rails. A pair of brake rails runs parallel to the guide rails and passes through each slide. Linear bearings are used between the brake block and guide rails to reduce friction losses. The spring of the multimodal actuator can be interchanged to provide different stiffnesses, and the spring connects the power supply and load.

2.2. Design of the brake block

The three brake blocks are named brake blocks 1, 2, and 3, as shown in Fig. 1. The spring connects brake blocks 1 and 2, and the other end of brake block 2 is the nut of the ball screw. Brake block 3 mounts the rotational DC motor on one end and a ball screw on the other. Every brake block is controlled by a brake motor (RB-150CS) that engages or disengages the brake pads such that the brake block can be fixated or released with respect to the brake rails. The brake block mechanism is shown in Fig. 2. The brake motor rotates the gear, and the gear pushes the up and down movement of the rack. Then, the push plate moves forward or backward. In this manner, the brake block is fixated on the brake rails. Otherwise, the brake block is released from the brake rails.

2.3. Brake performance

Braking force is an important output performance measure of the brake block; thus, the brake block must be designed based on the brake force demand. The force analysis of the disengaged and engaged

https://doi.org/10.1017/S0263574716000576 Published online by Cambridge University Press

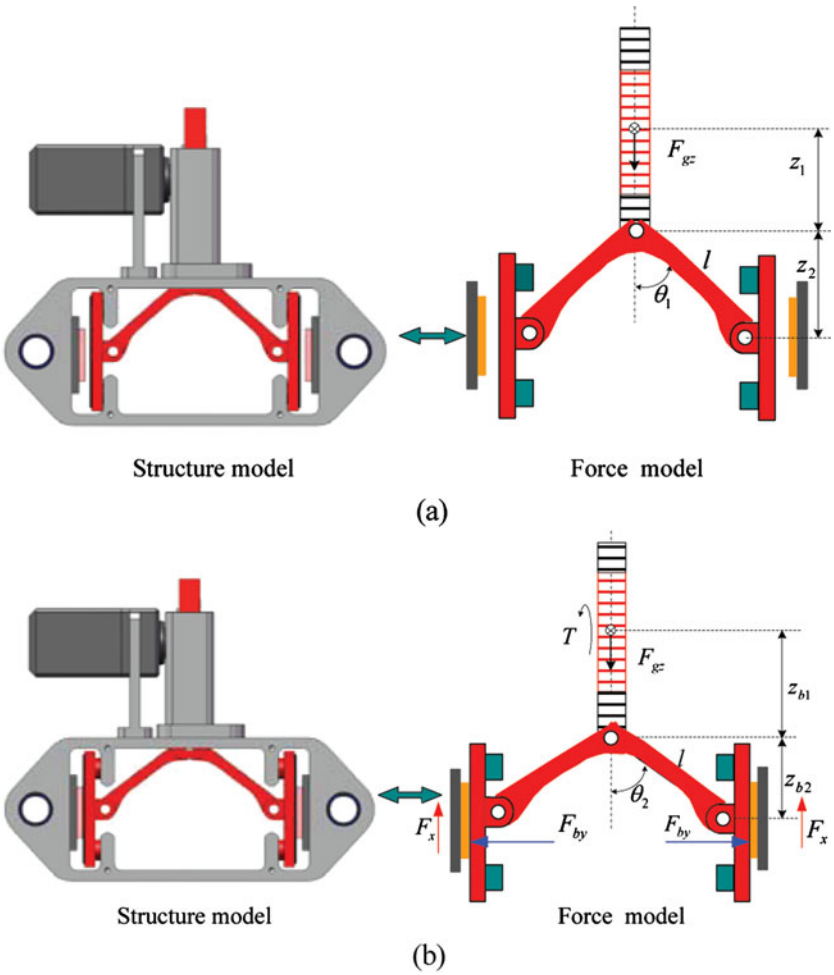

Fig. 3. (a) Force analysis of the disengaged brake block. (b) Force analysis of the engaged brake block.

brake block is shown in Fig. 3. When the brake block disengaged, the angle between the push rod and vertical line is θ_1, and the angle increased from θ_1 to θ_2 when the brake block changes from disengaged to engaged. The distance between the meshing centre of the gear and the hinged centre of the push rod is z_1, and the distance between the hinged centre of the push rod and the centre of the brake force is z_2 when the brake block is disengaged. However, the distance z_1 changes from z_1 to z_{b1} and the distance z_2 changes from z_2 to z_{b2} when the brake block is engaged. The desired braking force F_x can be used to express the Coulomb friction model when the brake block is engaged:

$$F_x = \mu \cdot F_{by} \tag{1}$$

where μ is the coefficient of kinetic friction and F_{by} is the maximum normal force of the push plate.

F_{by} is produced by the circumferential force of gear F_{gz}, which can be written as

$$F_{by} = F_{gz}\tan\theta_2 \tag{2}$$

The circumferential force of gear F_{gz} can be calculated with the torque of the brake motor T, the number of gear teeth n, and the module of the gear m:

$$F_{gz} = \frac{2T}{n \times m} \tag{3}$$

https://doi.org/10.1017/S0263574716000576 Published online by Cambridge University Press

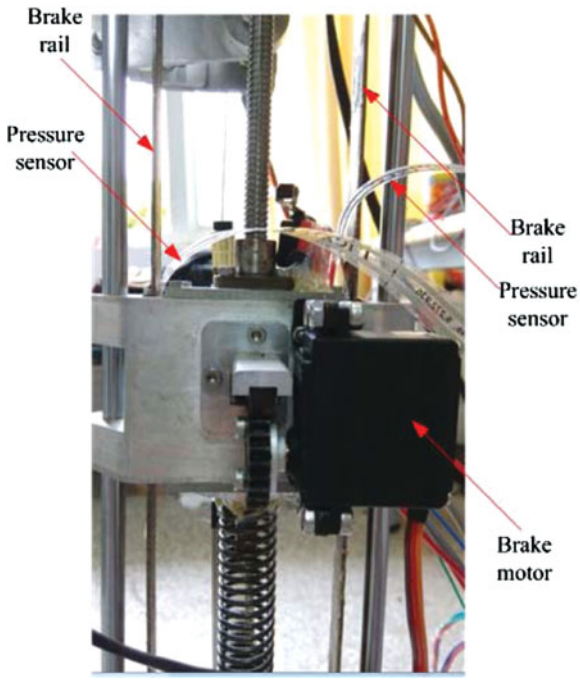

Fig. 4. Testing of the braking force.

When the brake block changes from disengaged to engaged, the displacement deformation of rack Δz can be written as

$$\Delta z = \frac{1}{2} n \times m \times \phi \tag{4}$$

where ϕ is the rotation angle of the brake motor.

The distance between the hinged centre of the push rod and the centre of the brake force z_{b2} when the brake block engaged is given by

$$z_{b2} = z_2 - \Delta z \tag{5}$$

Then, θ_2 can be derived by

$$\theta_2 = \cos^{-1}\left(\frac{z_{b2}}{l}\right) = \cos^{-1}\left(\frac{z_2 - \frac{nm}{2}}{l}\right) \tag{6}$$

With θ_2, the desired braking force F_x can be written as

$$F_x = \frac{2T\mu}{nm} \tan\left(\cos^{-1}\left(\frac{z_2 - \frac{nm}{2}}{l}\right)\right) \tag{7}$$

When the braking force required for the multimodal actuator is determined, the model selection of brake motor can be selected according to Eq. (7).

Experiments on the braking force were conducted to test the brake performance. The pressure sensor (FlexiForce sensor, 100 1 bs, 45 kg) was mounted onto the brake rail, as shown in Fig. 4. The brake motor was used to drive the push rod to a specified angle, and the relationship between the motor rotation angle and braking force is shown in Fig. 5. The brake block is disengaged when the brake motor is at 0^0, and the brake block is fully engaged when the brake motor is at 20^0. The time needed to move the brake motor through 20^0 is 0.33 s.

The results in Fig. 5 show that the mechanism can produce braking forces of up to approximately 75 N. The push plate starts to contact the brake rail from approximately 18^0 and above, and the brake

https://doi.org/10.1017/S0263574716000576 Published online by Cambridge University Press

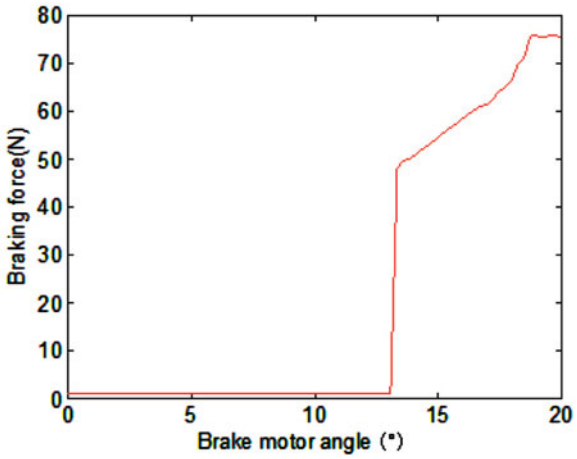

Fig. 5. Braking force vs. brake motor angle.

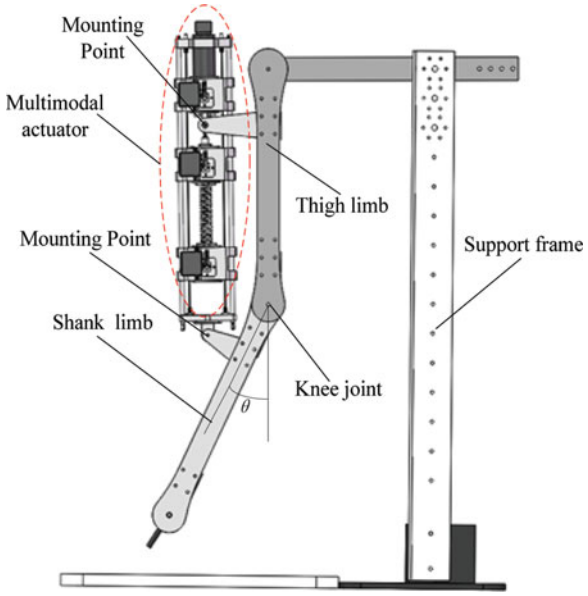

Fig. 6. Power-assisted knee exoskeleton.

block is fully engaged at approximately 20^0. The result shows that it is possible to control the braking force by controlling the brake motor angle, and the output of the braking force meets the requirement of the power-assisted knee exoskeleton.

3. Platform of the Power-assisted Knee Exoskeleton

3.1. Design of the power-assisted knee exoskeleton

Although significant advances have been made in exoskeleton robots, most of these robots are actuated by a motor and hydraulic system, and the sock-adsorption buffer function and energy utilization of these actuators are generally not very good. In this paper, the aim is to design an actuator for specific advantages, such as energy efficiency and compliance. The multimodal actuator is designed to actuate the rotary joint of the power-assisted knee exoskeleton, as shown in Fig. 6. Brake block 3 is mounted on the thigh limb as one mounting point, and the end of the guide rail is mounted on the shank limb as another mounting point. The distance between these two points is the output length of the actuator. The multimodal actuator allows the knee joint to be operated as human knee motion.

https://doi.org/10.1017/S0263574716000576 Published online by Cambridge University Press

Table. I. Motion modes of the power-assisted knee exoskeleton.

Name	Main motor	Brake block 1	Brake block 2	Brake block 3
(1) Initial state	–	0	0	0
	The shank limb is in contact with the ground. The initial angle between the shank limb and vertical direction is θ. The actuator is passive and completely free to move (as shown in Fig. 7(a)).			
(2) Flexion of the shank limb	1	0	1	0
	The motor rotates and drives the screw-nut mechanism. The distance between brake blocks 2 and 3 decreases, and the angle θ increases. The shank limb flexion is directly controlled by the motor, and precise control of the leg can be achieved during this stiff position controlled mode (as shown in Fig. 7(b)).			
(3) Extension of the shank limb	1	0	1	0
	Swing of the shank limb: The motor counter-rotates and drives the screw-nut mechanism. The distance between brake blocks 2 and 3 increases, and the angle θ decreases. The shank limb extends until it is in contact with the ground (as shown in Fig. 7(c)).			
	1	1	0	1
	Touched the ground flexibility: This state is that the pressure sensor mounted on the end of shank limb detects the increase in force. The motor rotates continuously, and the spring is attached to a motor in series to filter the instantaneous impact (as shown in Fig. 7(d)).			
	1	1	0	0
	The energy is stored: The motor rotates continuously, and the spring is compressed until maximum compression is achieved. This mode allows energy to be stored in the spring for energy-efficient motor control (as shown in Fig. 7(e)).			
(4) Release of the spring energy	1	1	0	0
	The motor counter-rotates rapidly. The storing kinetic energy is released. The shank limb is bounced. This mode allows the actuator to increase its power output (as shown in Fig. 7(f)).			
(5) Flexion of the shank limb again	1	0	1	0
	Brake block 1 is disengaged, and brake block 2 is engaged after releasing the spring energy. The motor rotates, and the angle θ increases. Flexion of the shank limb occurs again (as shown in Fig. 7(b)).			

Because the multimodal actuator is used for knee joint motion, hip and ankle motion is not considered, and the thigh limb is fixed. The three brake blocks of the multimodal actuator can switch between two discrete states, engaged or disengaged, so many modes of power-assisted knee exoskeleton are possible.

These modes are illustrated in Table I and Fig. 7. For the brake block, "0" and "1" indicate disengaged and engaged, respectively, and for the motor, "1" and "0" indicate actuated and unactuated, respectively.

3.2. Modeling of the power-assisted knee exoskeleton

The model of power-assisted knee exoskeleton is shown in Fig. 7(a). The motor is mounted at brake block 3 and fixed on the thigh limb. Brake block 3 have a mass m_3 and do not move. Brake blocks 2 and 1 have masses m_2 and m_1 at positions x_2 and x_1, respectively. At the output of the actuator, the position of the load is denoted by x_l, and when driving a shank limb with a mass that includes the frame and rails of the actuator m_l, the three degrees of freedom are described by three equations of

https://doi.org/10.1017/S0263574716000576 Published online by Cambridge University Press

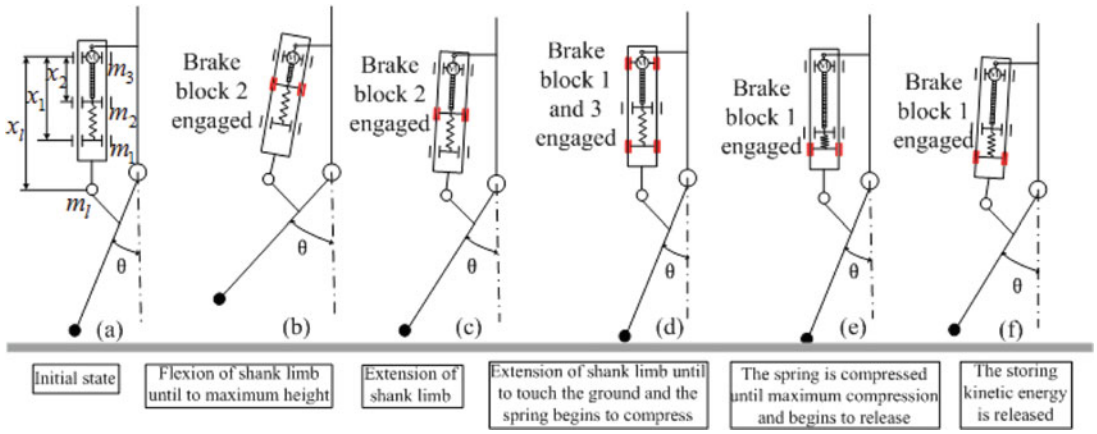

Fig. 7. Different modes during a motion cycle.

motion:

$$m_2\ddot{x}_2 + k_s(x_2 - x_1) + f_2 = F_M \tag{8}$$

$$m_1\ddot{x}_1 + k_s(x_1 - x_2) + f_1 = 0 \tag{9}$$

$$m_l\ddot{x}_l + f_2 + f_1 + f_3 = 0 \tag{10}$$

where k_s is the coefficient of the spring. F_M is the force provided by the motor. f_1, f_2, and f_3 are the friction force from brake blocks 1–3, respectively.

The friction from the brake block results in a nonlinear system with discontinuities during the power-assisted knee exoskeleton motion cycle, and thus, such a system is difficult to model. When the brake block is engaged, the brake block is no longer moving, and the friction force of the brake block is subject to static friction. Combining this static friction in one or more brake blocks allows the actuator to switch between discrete states in which the equations of motion can be reduced and simplified.

When the power-assisted knee exoskeleton moves from its initial state (Fig. 7(a)), flexion of the shank limb to the maximum height (Fig. 7(b)), to extension of the shank limb (Fig. 7(c)), brake block 2 is engaged and brake block 1 is not moving on the rail, which is stiff position control mode. The motor force directly affects the output, and the inertia from brake blocks 1 and 2 are added to the load:

$$F_M = (m_2 + m_1 + m_l)\ddot{x}_l \tag{11}$$

When the power-assisted knee exoskeleton moves from the shank limb touching the ground (Fig. 7(d)), the spring is compressed (Fig. 7(e)). The stored kinetic energy is released (Fig. 7(f)), and brake block 1 is engaged, which is in the series elastic actuation control mode. The mass of brake block 1 is added to the load:

$$(m_1 + m_l)\ddot{x}_l + k_s(x_l - x_2) = 0 \tag{12}$$

$$m_2\ddot{x}_2 + k_s(x_2 - x_l) = F_m \tag{13}$$

If the motor provides a position input $r(t) = x_2(t)$ instead of a force input and considering the damping of the system (damping coefficient c_s), Eq. (12) can be written as

$$(m_1 + m_l)\ddot{x}_l + k_s x_l + c_s\dot{x}_l = k_s r(t) + c_s\dot{r}(t) \tag{14}$$

https://doi.org/10.1017/S0263574716000576 Published online by Cambridge University Press

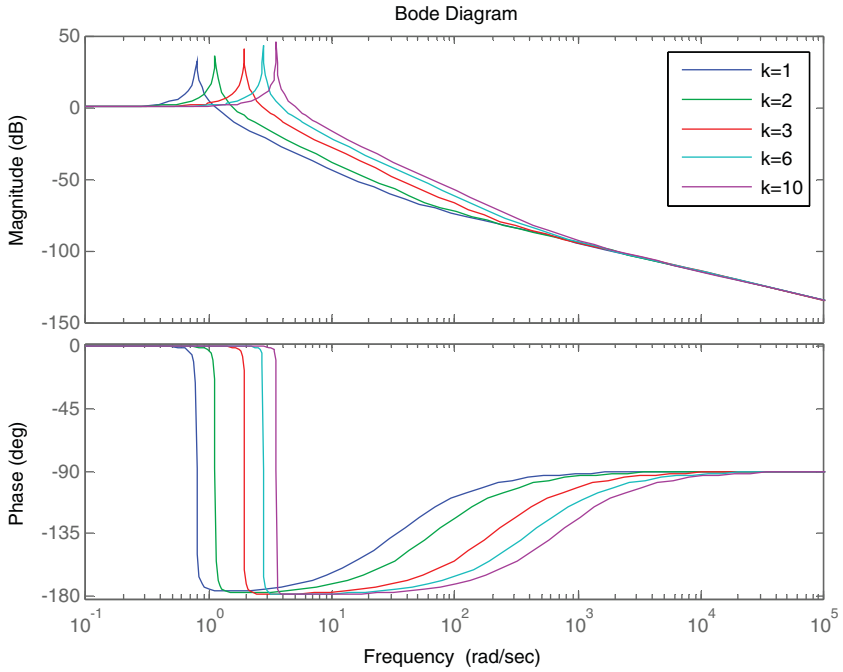

Fig. 8. Bode plot of the open-loop response of the actuator with different spring coefficients.

Laplace transform is used to combine the output and input:

$$\frac{X_l(s)}{R(s)} = \frac{c_s s + k_s}{(m_1 + m_l)s^2 + c_s s + k_s} \tag{15}$$

Simulation studies were conducted to study the effect of different spring coefficients and damping coefficients for control system performance. Figure 8 shows the open-loop bode diagram of the power-assisted exoskeleton's series elastic mode for a number of spring coefficients, where $k_s = 1\,\mathrm{N/mm}$, $2\,\mathrm{N/mm}$, $3\,\mathrm{N/mm}$, $6\,\mathrm{N/mm}$, and $10\,\mathrm{N/mm}$. The values for m_1 and m_l are taken from the experimental setup, $m_1 = 0.299\,\mathrm{kg}$ and $m_l = 1.21\,\mathrm{kg}$. The damping coefficient is $c_s = 1\,\mathrm{Ns/mm}$. The plots show that the gain margin and phase margin can allow for system control with guaranteed stability and better dynamic characteristics. Figure 8 also shows that the phase margin gradually decreases with increases in the spring coefficient, and the magnitude has a larger resonance peak when the spring coefficient increases to $10\,\mathrm{N/mm}$.

Figure 9 shows the open-loop bode diagram of the power-assisted exoskeleton's series elastic mode for a number of damping coefficients, where $c_s = 1\,\mathrm{Ns/mm}$, $0.5\,\mathrm{Ns/mm}$, $0.05\,\mathrm{Ns/mm}$, $0.015\,\mathrm{Ns/mm}$, and $0.005\,\mathrm{Ns/mm}$. The spring coefficient is $k_s = 1\,\mathrm{N/mm}$. Figure 9 shows that the phase margin gradually increases with increases in the damping coefficient and the stabilization of system increased. With increasing of the damping coefficient, the resonance peak decreases, and the step response overshoot is also smaller. Thus, it can be drew a conclusion that the larger damping coefficient is favorable for the stability of the system.

Figure 10 shows the close-loop bode diagram of the power-assisted exoskeleton's series elastic mode for a number of spring coefficients, where $k_s = 1\,\mathrm{N/mm}$, $2\,\mathrm{N/mm}$, $3\,\mathrm{N/mm}$, $6\,\mathrm{N/mm}$, and $10\,\mathrm{N/mm}$.

Figure 10 shows that the gain margin and phase margin can allow for system control with guaranteed stability. Figure 10 also shows that the phase margin gradually decreases with increases in the spring stiffness, and the amplitude and the phase following characteristic of the system gradually improve with increasing of the stiffness.

Figure 11 shows the close-loop bode diagram of the power-assisted exoskeleton's series elastic mode for a number of damping coefficients, where $c_s = 1\,\mathrm{Ns/mm}$, $0.5\,\mathrm{Ns/mm}$, $0.05\,\mathrm{Ns/mm}$, $0.015\,\mathrm{Ns/mm}$, and $0.005\,\mathrm{Ns/mm}$. The spring coefficient is $k_s = 1\,\mathrm{N/mm}$.

https://doi.org/10.1017/S0263574716000576 Published online by Cambridge University Press

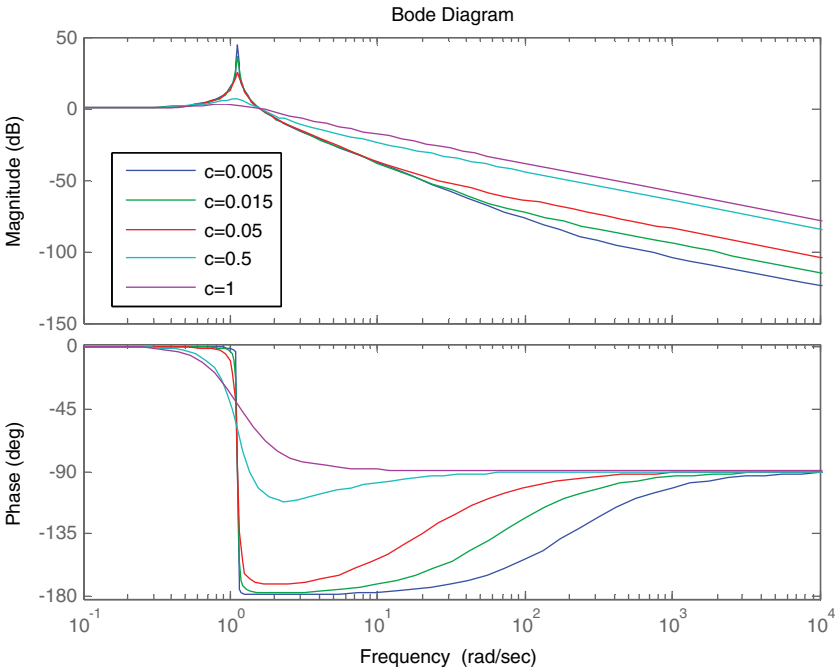

Fig. 9. Bode plot of the open-loop response of the actuator with different damping coefficients.

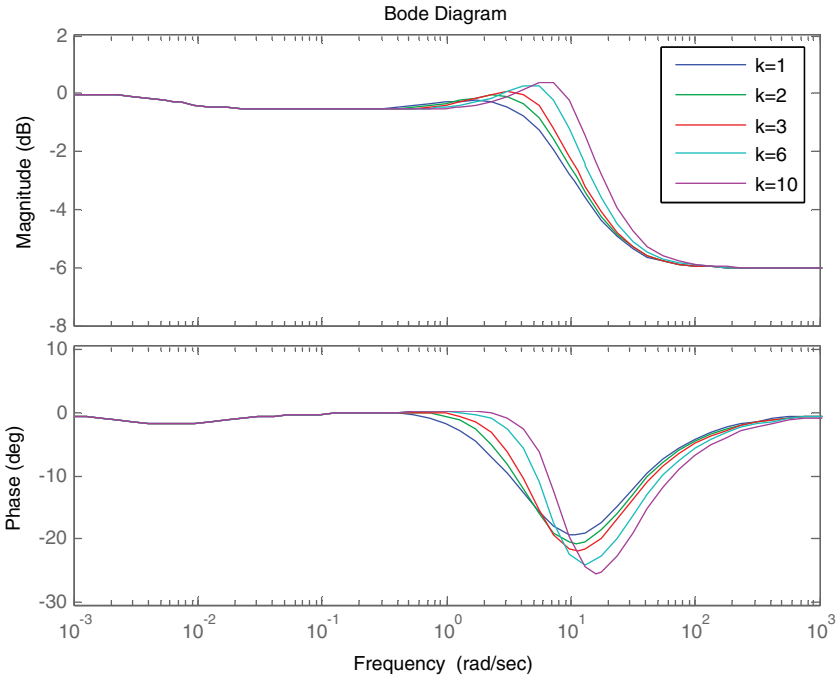

Fig. 10. Bode plot of the close-loop response of the actuator with different spring coefficients.

Figure 11 shows that the gain margin and phase margin can allow for system control with guaranteed stability. Figure 11 also shows that the phase margin increases gradually with increases in the damping coefficient, and the stability of the elastic actuator system gradually improves with increasing of the damping coefficient.

https://doi.org/10.1017/S0263574716000576 Published online by Cambridge University Press

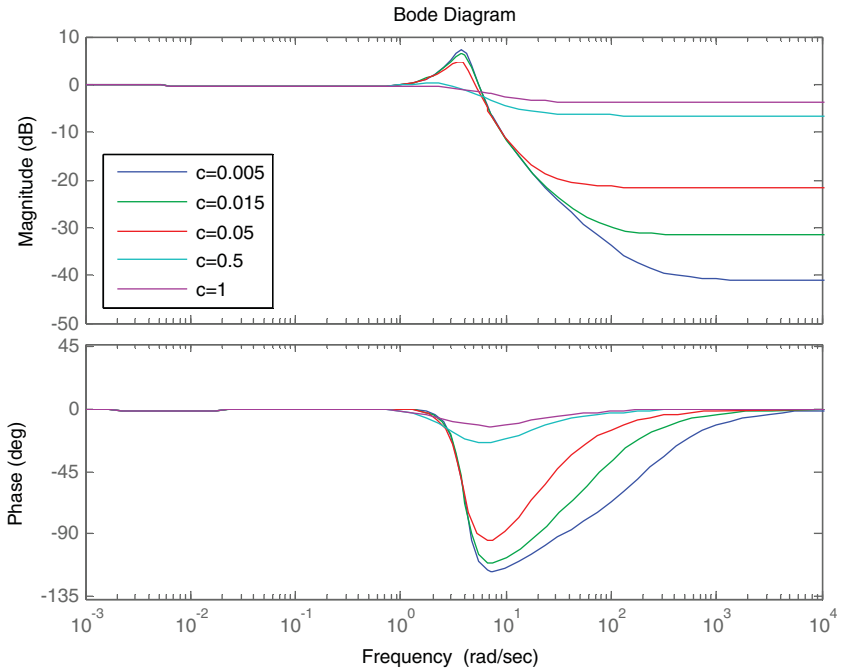

Fig. 11. Bode plot of the close-loop response of the actuator with different damping coefficients.

4. Experiments and Analysis

The power-assisted exoskeleton is designed to assist the knee joint motion, but for the safety of the wearer, the motion control strategy was first implemented and tested on the robotic exoskeleton platform. Also, the movement following effect of the exoskeleton was tested, that is, the human walks independently (without wearing the exoskeleton), and the power-assisted knee exoskeleton was tested following the human motion synchronously. This section presents the experiments and results.

4.1. Control strategy

The electronics of a power-assisted exoskeleton consist of drivers with a power supply for the knee, a brake motor, sensors, microcontrollers, and a host PC. For the motor drivers, MAXON EPOS2 50/5 is employed, which were also used as the interface to analogue sensors in the power-assisted exoskeleton prototype. One rotational potentiometer is installed at the knee axis to measure the angle of the knee joint. Two linear potentiometers are installed on the brake blocks, with one to measure the distance between brake blocks 1 and 2 and the other to measure the distance between brake blocks 2 and 3. One pressure force sensor is installed at the end of the shank limb to measure the reaction force between the exoskeleton leg and ground. A signal acquisition card for the displacement sensor and force sensor based on USB is designed, and the real-time data acquisition and data fusion are implemented on the PC. In the host computer, Studio Visual 2013 software and C language are used for programming. Then, the control procedure is performed.

The knee actuator is controlled using the "Position mode" of the EPOS controllers. The control strategy can be achieved by a state machine, as shown in Fig. 12. The state machine consists of six states that can be represented by the three-bit information in Table II, and each bit indicates the output/no output of the pressure force sensor, retract/protract of the screw-nut, and engage/disengage of brake block 1, respectively. The power-assisted knee exoskeleton starts with the "initial state" (labeled as "100" in Fig. 12), in which the shank limb is in contact with the ground and the actuator is passive, as shown in Fig. 13(a). Then, brake block 2 is engaged, and brake blocks 1 and 3 are disengaged. The motor rotates and drives the screw-nut mechanism, and the shank limb is in flexion (i.e., the "000" state), as shown in Fig. 13(b). The motor rotates continuously, and the motor controls the knee joint to retract the leg until the shank limb reaches the maximum height (i.e., the "001" state), as shown in Fig. 13(c). The motor counter-rotates and drives the screw-nut mechanism when the shank limb flexes until the maximum height is reached, and the shank limb is in extension (i.e., the "010"

https://doi.org/10.1017/S0263574716000576 Published online by Cambridge University Press

Table II. Variables of the state machine for the control of the power-assisted knee exoskeleton.

Label	Object	State
0_ _	The output of the pressure force sensor	No output
1_ _	The output of the pressure force sensor	Output
_0_	Screw-nut	Retracted
_1_	Screw-nut	Protracted
_ _ 0	Brake block 1	Disengaged
_ _ 1	Brake block 1	Engaged

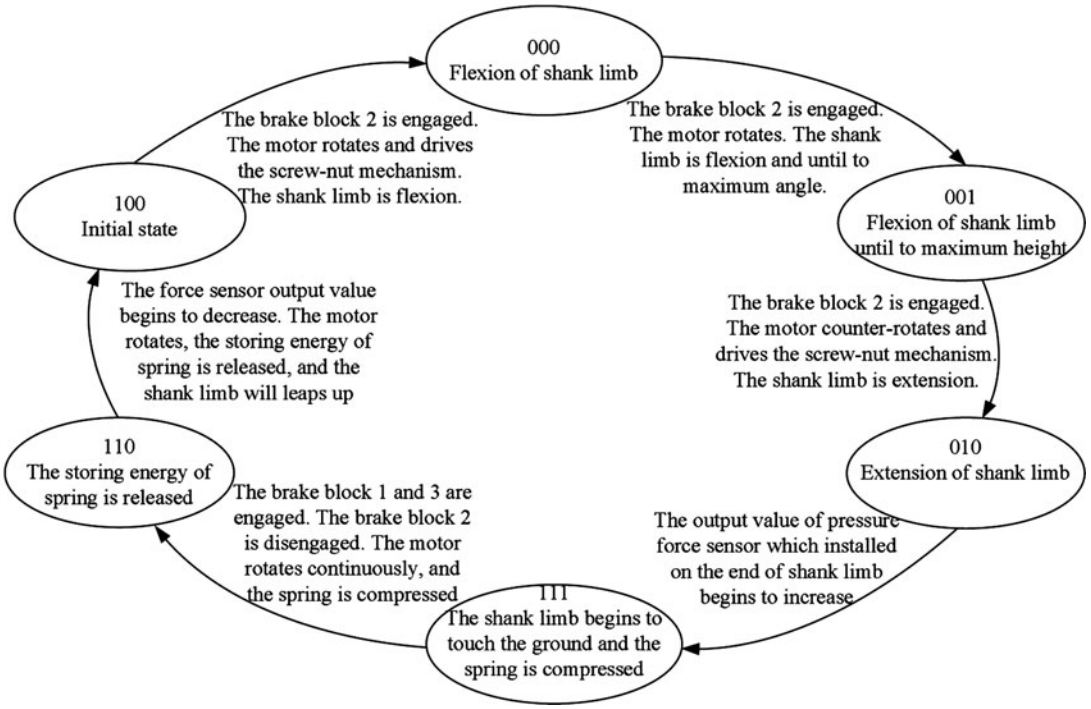

Fig. 12. State machine diagram for the control of the power-assisted knee exoskeleton.

state), as shown in Fig. 13(d). When the shank limb extends continuously and begins to touch the ground, which triggers the "111" state, as shown in Fig. 13(e), the spring begins to be compressed and the pressure force sensor begins to output the force. The motor rotates continuously, and the spring is compressed until maximum compression is achieved. Then, the motor counter-rotates rapidly, the storing kinetic energy is released, and the shank limb is bounced (i.e., the "110" state), as shown in Fig. 13(f).

4.2. Testing of the power-assisted knee exoskeleton

The shank limb of the power-assisted knee exoskeleton was driven to motion with a Maxon motor when the control program began to run. The pressure force sensor signal and angle sensor signal of the knee joint were acquired with the data acquisition system in real-time. The positive and negative rotation of the Maxon motor and the start and stop of the brake motor were implemented according to the sensor signals, and then, the engagement and disengagement of different brake blocks were operated and the motion modes of power-assisted knee exoskeleton were realized during a stride cycle.

Figure 14 shows the motion pattern output of the power-assisted knee exoskeleton. From Fig. 14(a), the knee joint reaches the maximum flexion angle at approximately 0.6 s, and the distance between brake blocks 1 and 2 is minimum at this moment, as shown in Fig. 14(c). At the same time, the Maxon motor begins to counter-rotate the output torque of the motor from positive to negative at 0.6 s, as shown in Fig. 14(e). The knee joint reaches the maximum extension angle at approximately

https://doi.org/10.1017/S0263574716000576 Published online by Cambridge University Press

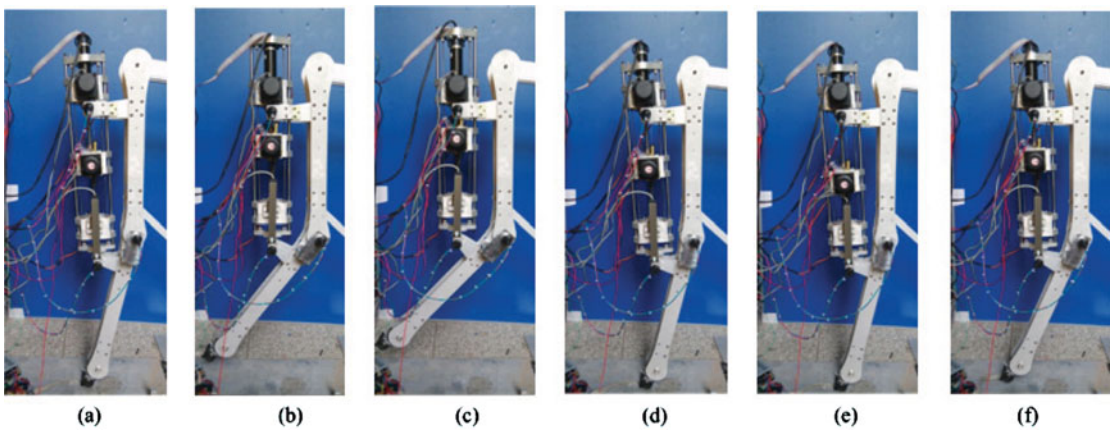

Fig. 13. Action sequences of the power-assisted exoskeleton during a motion cycle.

1.2 s (Fig. 14(a)). At this moment, the spring is compressed and reaches maximum compression, so the output force of the pressure force sensor attains the maximum value, as shown in Fig. 14(b). At the same time, brake block 2 begins to disengage and brake blocks 1 and 3 begin to engage; as a result, the torque of brake motor 2 begins to decrease, and the torque of brake motors 1 and 3 begin to increase, as shown in Fig. 14(f)–(h). The distance of brake blocks 2 and 3 also begin to decrease at approximately 1.2 s, as shown in Fig. 14(d).

4.3. Testing of the power-assisted knee exoskeleton following human motion

The power-assisted knee exoskeleton must keep pace with the human body and follow the movement of the human body to provide adequate assistance. The movement-following effect of the exoskeleton was tested. For the safety of the wearer, the wearer did not wear the exoskeleton directly but walked independently, and the power-assisted knee exoskeleton was tested following the wearer motion synchronously. The wearer wore the auxiliary device for knee angle measurement and the in-shoe plantar, as shown in Fig. 15. The angle sensor and pressure sensor collected the human motion, and these signals were used to control the power-assisted knee exoskeleton following the human motion synchronously. The motion sequences of the power-assisted exoskeleton following the human motion are shown in Fig. 16, and the knee joint angle curves of the power-assisted exoskeleton and human are shown in Fig. 17. As Fig. 17 shows, the power-assisted exoskeleton has a good following motion and the angle error of the knee exoskeleton followed the human motion is not more than 0.4°.

5. Conclusions

A multimodal actuator achieving the effective drive demand of a power-assisted knee exoskeleton is developed. The actuator switched between different modes of operation through the motor driving the screw nut in series with a spring in combination with three brake blocks. The design of a suitable brake block is the key to the multimodal actuator, which is able to generate sufficient braking force with physical dimensions that are sufficiently compact to be mounted in the power-assisted knee exoskeleton. A prototype of the multimodal actuator was designed and tested. The brake block was controlled by a brake motor that engages or disengages the brake pads such that the brake block can be fixated or released with respect to the brake rails. The brake motor rotates the gear, which pushes the up and down movement of the rack. When the rack moves down, the brake pad is pushed against the brake rail. In this manner, the brake block is fixated on the brake rails. Otherwise, the brake block is released by the brake rails. The brake block can produce a braking force of 75 N with a switching time of approximately 0.33 s. The output of the braking force meets the requirement of the power-assisted knee exoskeleton.

A power-assisted knee exoskeleton prototype based on the multimodal actuator was constructed. The motion modes during a stride cycle were analyzed, the effects of different spring and damping coefficients for control system performance were simulated, and an experiment on the power-assisted knee exoskeleton following human motion was implemented. The central controller converts the

https://doi.org/10.1017/S0263574716000576 Published online by Cambridge University Press

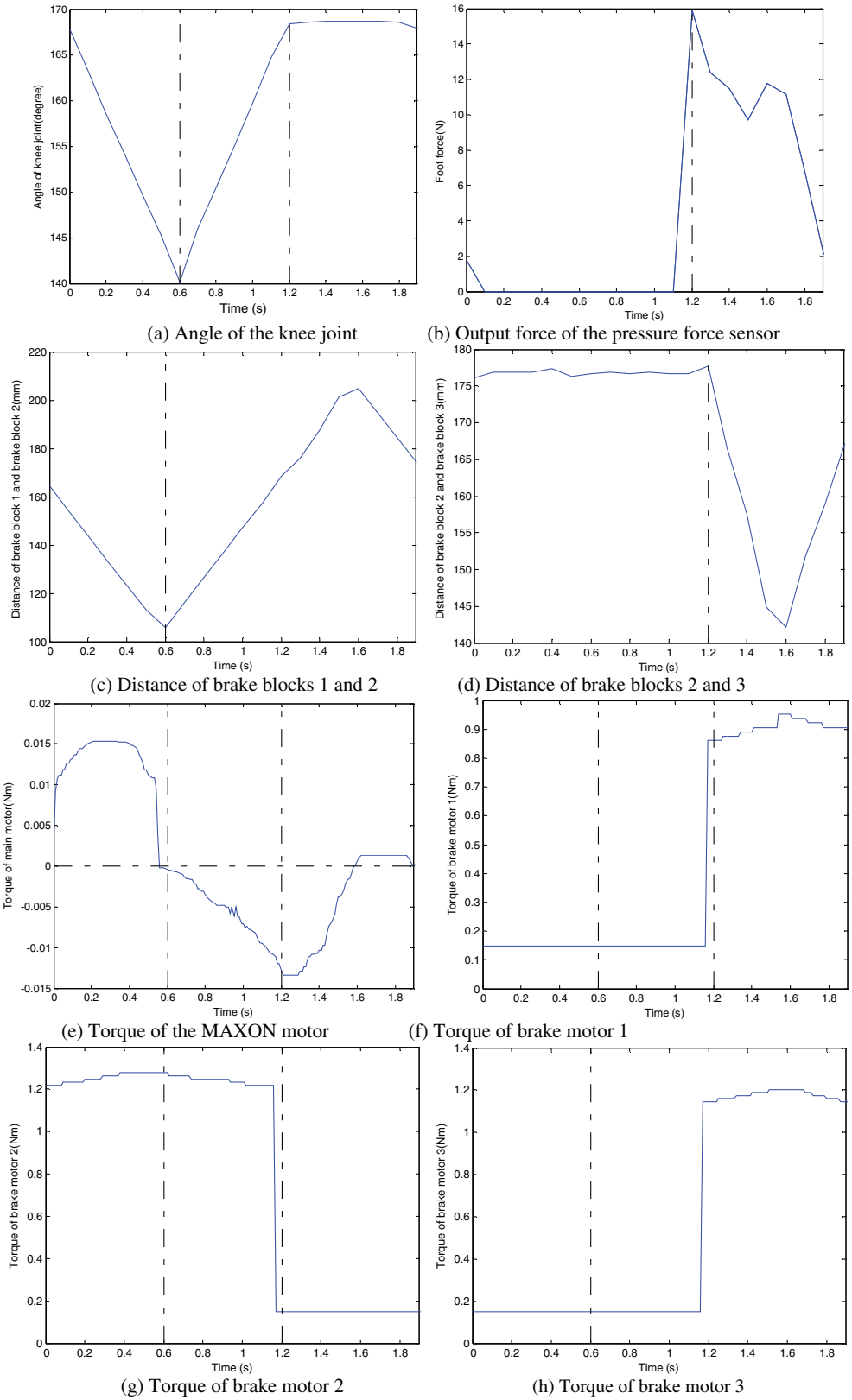

(a) Angle of the knee joint (b) Output force of the pressure force sensor

(c) Distance of brake blocks 1 and 2 (d) Distance of brake blocks 2 and 3

(e) Torque of the MAXON motor (f) Torque of brake motor 1

(g) Torque of brake motor 2 (h) Torque of brake motor 3

Fig. 14. Motion pattern output of the power-assisted knee exoskeleton. (a) Angle of the knee joint. (b) Output force of the pressure force sensor. (c) Distance of brake blocks 1 and 2. (d) Distance of brake blocks 2 and 3. (e) Torque of the MAXON motor. (f) Torque of brake motor 1. (g) Torque of brake motor 2. (h) Torque of brake motor 3.

https://doi.org/10.1017/S0263574716000576 Published online by Cambridge University Press

Fig. 15. Sensors worn on the tester.

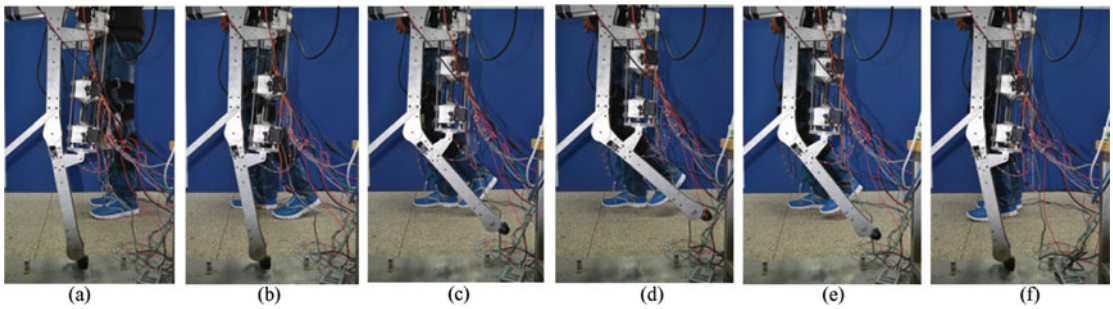

Fig. 16. Motion sequences of the power-assisted exoskeleton following the human motion.

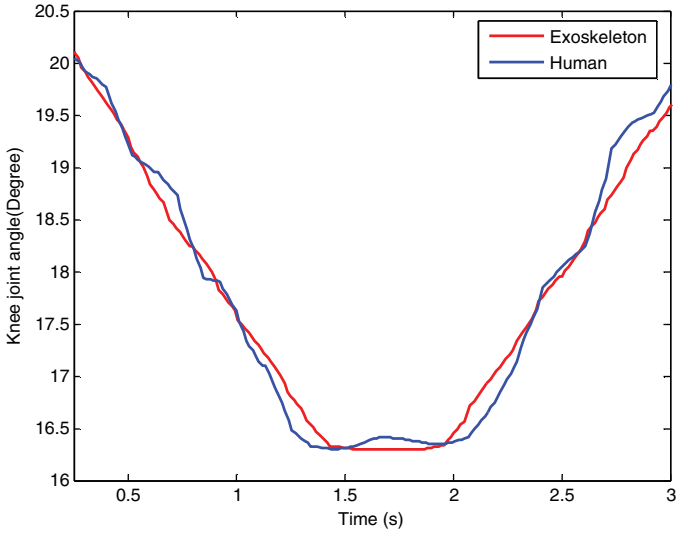

Fig. 17. Knee joint angle of the power-assisted knee exoskeleton and human.

https://doi.org/10.1017/S0263574716000576 Published online by Cambridge University Press

human motion signal from pressure force sensors and joint angle sensors into the control signal for the power-assisted knee exoskeleton driving system, and the sensor-system collects the motion signal, which forms a closed-loop control for controlling the exoskeleton. The results showed that the angle error of the knee exoskeleton followed the human motion is not more than 0.4˚, and the response time error of the knee exoskeleton followed the human motion is not more than 0.2 s. The power-assisted knee exoskeleton was only tested following the human motion; thus, future research will investigate the effect of exoskeleton-generated assistance when wearing the exoskeleton during motion. The brake blocks are a key component of the multimodal actuator, and increasing the braking performance will have a significant effect on the amount of energy that can be stored in the spring. However, the braking force of our multimodal actuator prototype is not sufficiently large for large load masses. Thus, future studies will investigate better braking models. In addition, the weight and physical dimensions of the power-assisted knee exoskeleton prototype are large because the multimodal actuator is heavy and large. Therefore, there is also a plan to investigate light and high-efficiency design principles for the multimodal actuator.

Acknowledgements

This work is supported by the National Natural Science Foundation of China (Grant No. 51205182), the Natural Science Foundation of Jiangsu Province of China (Grant No. BK2012474) and the Innovation Foundation of NJIT (Grant No.CKJA 201501, JXKJ201510).

References

1. A. M. dollar and H. Herr, "Lower extremity exoskeleton and active orthoses: challenges and state-of-the-art," *IEEE Trans. Robot.* **24**(1), 144–158 (Jan. 2008).
2. M. M. Maria, C. P. Santos, A. Frizera-Neto, and R. Ceres, "Assistive mobility devices focusing on smart walkers: classification and review," *Robot. Auton. Syst.* **60**(4), 548–562 (Apr. 2012).
3. S. Viteckova, P. Kutilek and M. Jirina, "Wearable lower limb robotics: A review," *Biocybernetics Biomed. Eng.* **33**(2), 96–105 (Mar. 2013).
4. A. Zoss, H. Kazerooni and A. Chu, "Biomechanical design of the berkeley lower extremity exoskeleton," *IEEE/ASME Trans. Mechatronics* **11**(2), 128–138 (Apr. 2006).
5. S. Karlin, "Raiding Iron man's closet," *IEEE Spectrum* **48**(8), 25 (Aug. 2011).
6. C. J. Walsh, K. Pasch and H. Herr, "An Autonomous, Underactuated Exoskeleton for Load-Carrying Augmentation," *2006 IEEE/RSJ International Conference on Intelligent Robots and Systems*, Beijing, China (Oct. 2006) pp. 1410–1415.
7. G. Colombo, M. Joerg, R. Schreier and V. Dietz, "Treadmill training of paraplegic patients using a robotic orthosis," *J. Rehabil. Res. Develop.* 37(6), 693–700 (Feb. 2000).
8. M. Bortole, A. Venkatakrishnan, F. Zhu, J. C. Moreno, G. E. Francisco, J. L. Pons and J. L. Contreras-Vidal, "The H2 robotic exoskeleton for gait rehabilitation after stroke: Early findings from a clinical study," *J. NeuroEngineering Rehabil.* 12 54 (2015). DOI: 10.1186/s12984-015-0048-y.
9. S. K. Banala, S. K. Agrawal, S. H. Kim and J. P. Scholz, "Novel gait adaptation and neuromotor training results using an active leg exoskeleton," *IEEE/ASME Trans. Mechatronics* **15**(2), 216–225 (Apr. 2010).
10. C. Copilusi, M. Ceccarelli and G. Carbone, "Design and numerical characterization of a new leg exoskeleton for motion assistance," *Robotica* 33, 1147–1162 (2015).
11. H. Kawamoto and Y. Sankai, "Comfortable Power Assist Control Method for Walking Aid by HAL-3," *2002 IEEE International Conference on Systems, Man and Cybernetics*, Vol. 4, Ibaraki, Japan (Oct. 6–9, 2002) p. 6.
12. G. A. Pratt and M. M. Williamson, "Series Elastic Actuators," *1995 IEEE/RSJ International Conference on Intelligent Robots and Systems*, vol. 1, Pittsburgh, PA, USA (Aug 5-9, 1995) pp. 399–406.
13. M. Ahmadi and M. Buehler, "Stable control of a simulated one-legged running robot with hip and leg compliance," *IEEE Trans. Robot. Autom.* **13**(1), 96–104 (Mar. 1997).
14. D. Paluska and H. Herr, "The effect of series elasticity on actuator power and work output: Implications for robotic and prosthetic joint design," *Robot. Auton. Syst.* **54**(8), 667–673 (Aug. 2006).
15. R. Schiavi, G. Grioli, S. Sen and A. Bicchi, "VSA-II: A Novel Prototype of Variable Stiffness Actuator for Safe and Performing Robots Interacting with Humans," *2008 IEEE International Conference on Robotics and Automation*, Pasadena, CA, USA, (May 19–23, 2008) pp. 2171–2176.
16. A. Jafari, N. G. Tsagarakis, B. Vanderborght and D. G. Caldwell, "A Novel Actuator with Adjustable Stiffness (AwAS)," *2010 IEEE/RSJ International Conference on Intelligent Robots and Systems (IROS)*, Taipei, Taiwan, (18–22 Oct, 2010) pp. 4201–4206.
17. J. Choi, S. Hong, W. Lee, S. Kang and M. Kim, "A robot joint with variable stiffness using leaf springs," *IEEE Trans. Robot.* **27**(2), 229–238 (Feb. 2011).

18. B. S. Kim, J. B. Song and J. J. Park, "A serial-type dual actuator unit with planetary gear train: Basic design and applications," *IEEE/ASME Trans. Mechatronics* **15**(1), 108–116 (Feb. 2010).
19. A. Jafari, N. Tsagarakis and D. Caldwell, "Exploiting Natural Dynamics for Energy Minimization using an Actuator with Adjustable Stiffness (AwAS)," *2011 IEEE International Conference on Robotics and Automation (ICRA)*, Shanghai, China, (May 9–13, 2011) pp. 4632–4637.
20. J. W. Hurst, J. E. Chestnutt and A. A. Rizzi, "An actuator with Physically Variable Stiffness for Highly Dynamic Legged Locomotion," *2004 IEEE International Conference on Robotics and Automation (ICRA)*, New Orleans, LA, USA, (Apr. 26—May 1, 2004) pp. 4662–4667.
21. A. S. Shafer and M. Kermani, "On the feasibility and suitability of MR fluid clutches in human-friendly manipulators," *IEEE/ASME Trans. Mechatronics* **16**(6), 1073–1082 (Oct. 2011).
22. Y. Tenzer, B. L. Davies and F. Baena, "Four-state rotary joint control: Results with a novel programmable brake," *IEEE/ASME Trans. Mechatronics* **17**(5), 915–923 (May 2011).
23. B. Vanderborght, A. Albu-Schaeffer, A. Bicchi, E. Burdet, D. G. Caldwell, R. Carloni, M. Catalano, O. Eiberger, W. Friedl, G. Ganesh, M. Garabini, M. Grebenstein, G. Grioli, S. Haddadin, H. Hoppner, A. Jafari, M. Laffranchi, D. Lefeber, F. Petit, S. Stramigioli, N. Tsagarakis, M. Van Damme, R. Van Ham, L. C. Visser and S. Wolf, "Variable impedance actuator: A review," *Robot. Auton. Syst.* **61**(12), 1601–1614 (2013).
24. N. Tagliamonte, F. Sergi, D. Accoto, G. Carpino, E. Guglielmelli, "Double actuation architectures for rendering variable impedance in compliant robots: A review," *Mechatronics* **22**(8), 1187–1203 (2012).
25. D. Leach, F. Gunther, N. Maheshwari and F. Iida, "Linear multimodal actuation through discrete coupling," *IEEE/ASME Trans. Mechatronics* **19** (3), 827–839 (May 2013).
26. H. Yali, S. Aiguo, G. Haitao and Z. Songqing, "The muscle activation patterns of lower limb during stair climbing at different backpack load[J]," *Acta Bioeng. Biomech.* **17**(3), (2015). DOI:10.5277/ABB-00155-2014-06.